Icarus 319 (2019) 308–311

Contents lists available at ScienceDirect

Icarus

journal homepage: www.elsevier.com/locate/icarus

Latitudinal dependence of asteroid regolith formation by thermal fatigue

Maximilian Hamm[a,*], Hiroki Senshu[b], Matthias Grott[a]

[a] German Aerospace Center, Institute of Planetary Research, Berlin, Germany
[b] Chiba Institute of Technology, Planetary Exploration Research Center, Narashino, Japan

ARTICLE INFO

Keywords:
Asteroids
Surfaces
Regolith
Thermal histories

ABSTRACT

The latitudinal dependence of regolith formation by thermal fatigue is studied for variable solar declination and surface thermal inertia. We find that regolith generation takes place in a surprisingly wide band around the equator and make predictions for the regolith distribution on the target asteroids of the upcoming Hayabusa2 and OSIRIS-REx missions.

1. Introduction

The surface of asteroids consists of broken-up material called regolith, with constituent sizes varying from boulders to fine dust grains. Visiting spacecraft have characterized the texture of regolith covers in great detail, and a wealth of data has been returned from, e.g., Itokawa (Yano et al., 2006), Vesta (Jaumann et al., 2012), and Eros (Thomas et al., 2001). To understand the nature of the processes shaping these surfaces, it is crucial to understand the process of regolith formation, as it sets the stage for any subsequent surface evolution through, for example, regolith migration (Garcia et al., 2015). Recent studies have shown the importance of thermal fatigue as a regolith forming process (e.g. Molaro et al., 2015; 2017; Viles et al., 2010; Eppes et al., 2015), which could erode the surface faster than micrometeoroid impacts (Delbo et al., 2014; Dombard et al., 2010). However, the efficiency of this process as a function of latitude, solar declination and surface thermal inertia has not been well characterized to date.

Thermal fatigue describes the cracking and chipping of rocks by thermal stresses (e.g. Luque et al., 2011, Viles et al., 2010) and it results in the generation of fragments of ever decreasing size. Studies investigating thermal stresses in objects exposed to the space environment include comets (Kührt, 1984; Auger et al., 2018), meteoroids (Čapek et al., 2010 and 2012), boulders (Molaro et al., 2017) and granular microstructures (Molaro et al., 2015), and thermal fatigue is sometimes parameterized in terms of spatial or temporal temperature gradients (e.g. Auger et al., 2018; Molaro et al., 2017). However, while macroscopic temperature gradients can add to thermal fatigue on a macroscopic scale, the different thermal expansion of constituents can induce thermal fatigue on the microscopic scale, i.e. the individual grains constituting a boulder (Molaro et al., 2015). Molaro et al. (2015, 2017) demonstrated that in both cases the amplitude of the diurnal temperature wave is a more suitable proxy for the thermally induced breakdown of regolith.

This work will investigate the spatial distribution of thermal forcing on the target body rather than an actual thermo-mechanical fatigue model. The purpose is to understand the regolith distribution on a global scale rather than the breakdown of individual boulders. We assume that if thermal fatigue occurs at all, it will be strongest where the thermal forcing is strongest. To this end, we calculate the latitudes with the largest amplitude of the diurnal temperature curve as a representation of thermal stress. Results will show how these latitudes of maximum forcing change with thermal inertia and solar declination. We will then relate the results to C-type asteroid (162173) Ryugu, the target of the Hayabusa-2 mission (Tsuda et al., 2013; Müller et al., 2017), as well as B-type asteroid (101955) Bennu, the target of the OSIRIS-Rex mission (Lauretta et al., 2015).

2. Theory and methods

We calculate temperature profiles on a sphere solving the one-dimensional heat conduction equation for a homogeneous half-space using an explicit finite differences scheme (Takita et al., 2017). Temperatures are calculated on a grid with 250 nodes in depth for latitudes and longitudes varying in steps of one degree. The sphere is assumed to rotate with a period of 7.63 h and is placed at a fixed solar distance of 1.2 AU, corresponding to the rotational and orbital parameters of (162173) Ryugu (Müller et al., 2017). The influence of thermal inertia Γ and solar declination δ on the diurnal temperature amplitudes ΔT is calculated by studying their influence on the surface energy balance given by

* Corresponding author.
E-mail address: Maximilian.hamm@dlr.de (M. Hamm).

https://doi.org/10.1016/j.icarus.2018.09.033
Received 6 March 2018; Received in revised form 27 August 2018; Accepted 24 September 2018
Available online 25 September 2018

$$-\Gamma\sqrt{\frac{\pi}{P}}\frac{\partial T}{\partial z} = (1-A)I - \sigma\varepsilon T^4, \tag{1}$$

where P is the rotation period, A is albedo, σ the Stephan-Boltzmann constant, ε the emissivity, and z the depth normalized to the diurnal skin depth. It is worth noting that while we fix the rotational period to that of (162173) Ryugu in the following, Eq. (1) implies that the effects of rotation period and thermal inertia can compensate each other. Therefore, results presented below can be scaled to other rotation periods by adjusting the chosen thermal inertia.

Insolation I is given by

$$I(t) = \frac{I_0}{r_h^2}(\cos\phi\cos\delta\cos\psi(t) + \sin\phi\sin\delta), \tag{2}$$

where $I_0 = 1366.1\ \mathrm{W/m^2}$ is the solar constant at $1AU$, r_h is heliocentric distance, δ is solar declination, and ϕ is latitude with $\phi = 0$ at the equator. The local hour angle $\psi(t) = \omega t$ changes with time as the asteroid rotates and noon is defined by $\psi(t=0) = 0$. During nighttime I is set to zero.

The amplitude of the diurnal temperature variations is defined by $\Delta T = \frac{1}{2}(T_{max} - T_{min})$, where T_{max} and T_{min} are the maximum and minimum diurnal temperatures at the given location. The temperature rise during daytime is larger and faster than the cooling during the night, and the amplitude ΔT is thus generally dominated by the daytime temperature rise. It tends to increase towards the subsolar point $\phi = \delta$, where the maximum illumination

$$I_{max} = \frac{I_0}{r_h^2}\cos(\phi - \delta), \tag{3}$$

occurs. However, the length of the night remains a limiting factor. The larger the solar declination δ, the further north the sub-solar point and the shorter is the night, limiting the cooling of the surface. Due to the cosine dependence of the maximum illumination on the angle $\phi - \delta$, I_{max} changes only slowly near the subsolar point, but the length of the night sharply increases away from $\phi = \delta$. Consequently, the minimum diurnal temperature decreases towards lower latitudes, and ΔT reaches its maximum south of the subsolar latitude for δ larger than a critical value, ultimately limited by the boundary latitude of permanent insolation at $\phi = 90° - \delta$. Surfaces with high thermal inertia Γ react delayed to insolation changes, and large Γ reduces heating and cooling rates, which reduces the influence of short nights. Therefore, the amplitudes of the diurnal temperature curve ΔT will decrease with increasing Γ, and high Γ will shift the latitude of maximum amplitude towards higher latitudes.

3. Results

In the following, we will investigate the location of maximum temperature amplitude ΔT as a function of solar declination δ and thermal inertia. While solar declination will be varied between 0° and 85°, thermal inertia will be varied between 500 and 3000 J m^{-2} K^{-1} s$^{-1/2}$. These values cover the expected range of thermal inertia for various meteorites, ranging from 640 J K^{-1}m^{-2}s$^{-1/2}$ for CM2 chondrites to 3000 J K^{-1}m^{-2}s$^{-1/2}$ for E4 chondrites (Opeil et al., 2010). Non-chondritic materials like serpentine or enstatite also fall within this range. We choose the thermal inertia values to represent bulk material instead of unconsolidated material, as we want to estimate where thermal fatigue would be most likely to breakdown consolidated surface material.

As an example, the latitudinal distribution of temperature amplitudes ΔT is illustrated in Fig. 1, where a solar declination of $\delta = 45°$ and a thermal inertia of $\Gamma = 500$ J K^{-1}m^{-2}s$^{-1/2}$ have been assumed. The solid black line represents the equator and the subsolar latitude $\phi = \delta$ is indicated by the yellow line. The latitude ϕ_{max} of the maximum ΔT is represented in Fig. 1 by a solid white line. The dashed white lines represent the latitudes where 90% of the maximum ΔT is reached, and

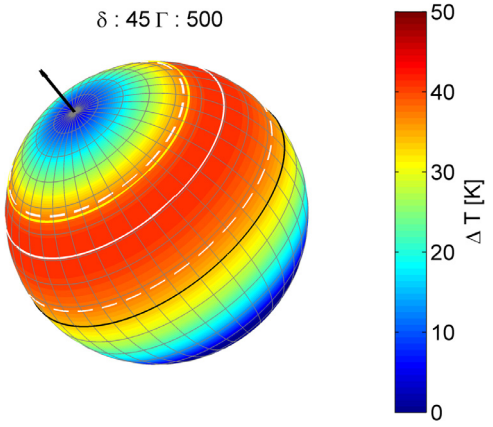

Fig. 1.. Amplitudes of diurnal temperature curves for a solar declination of $\delta = 45°$, and a thermal inertia of $\Gamma = 500$ J K^{-1}m^{-2}s$^{-1/2}$. The yellow line corresponds to the subsolar point $\phi = \delta$. The latitude of the maximum amplitude is represented by a solid white line, the dashed white lines indicate the latitude where $\Delta T = 0.9\ \Delta T_{max}$, and the solid black line represents the equator. (For interpretation of the references to color in this figure legend, the reader is referred to the web version of this article.)

these span a band of about ± 20° in latitude. This should correspond to the region in which most of the thermal fatigue can be expected, and it covers a significant fraction of the northern hemisphere. The 90% band is truncated in the north by the line of permanent insolation, which for $\delta = 45°$ coincides with the subsolar latitude. It is worth noting that for low solar declination, the 90% band widens to up to ± 30°, while for large δ the band can narrow down to ± 5°. Furthermore, large thermal inertia Γ would also cause slightly narrower bands (not shown).

Results for the entire range of considered parameters are shown in Fig. 2, which shows the maximum latitude ϕ_{max} for the diurnal temperature amplitude as a function of solar declination δ and thermal inertia Γ. The subsolar latitude $\phi = \delta$ as well as the area of permanent insolation are indicated for reference and the magnitude of ΔT_{max} is shown in color. As expected, ΔT_{max} is larger for lower δ and Γ.

The latitude ϕ_{max} of maximum temperature amplitude closely

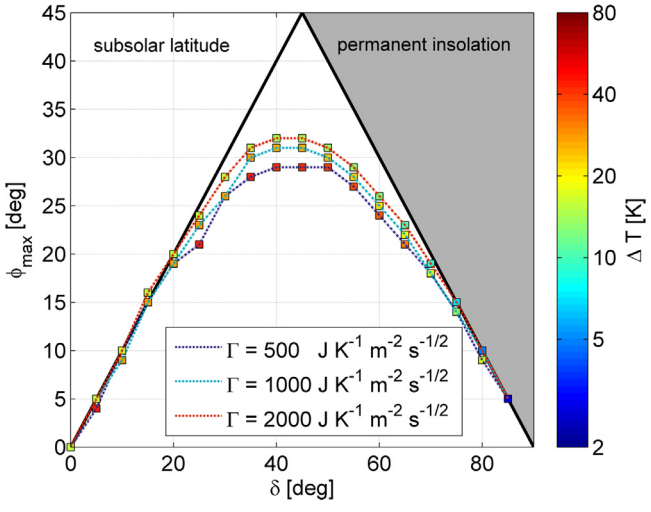

Fig. 2.. Latitude ϕ_{max} of the maximum diurnal temperature amplitude ΔT_{max} as a function of solar declination δ and thermal inertia Γ. The color indicates the magnitude; the grey area indicates the latitudes with permanent insolation depending on solar declination. Results for $\Gamma = 3000$ J K^{-1}m^{-2}s$^{-1/2}$ are not shown since they are indistinguishable from $\Gamma = 2000$ J K^{-1}m^{-2}s$^{-1/2}$. (For interpretation of the references to color in this figure legend, the reader is referred to the web version of this article.)

follows the subsolar latitude up to $\delta = 30°$. From there on, the increase of ϕ_{max} flattens, reaching its maximum of 29° to 32° at $\delta = 45°$. For larger solar declination ϕ_{max} decreases again, following the boundary of permanent insolation in accordance with the theoretical expectations discussed in Section 2. It is worth noting that ϕ_{max} is almost independent of Γ which has its strongest influence at solar declinations close to 45°, where the cooling rate is most significant due to the short night as discussed in Section 2.

4. Conclusions

The amplitude of the diurnal variation of the surface temperature can drive thermal fatigue on asteroids, and we have calculated thermophysical models for C-type asteroid (162173) Ryugu to determine the latitudes at which the diurnal temperature amplitudes become maximal. These are assumed to be representative for thermal stresses on the macroscopic and microscopic scales. The presented work encompasses a broad range of pole orientations and regolith compositions. Furthermore, Eq. (1) implies that our results can be applied to other rotation periods by scaling the thermal inertia appropriately.

The thermal stress field is a superposition of contributions from microscopic and macroscopic stresses, which in turn are to first order proportional the temperature amplitude (Molaro et al., 2015, 2017; online methods Delbo et al., 2014). However, stress concentrations will occur at cracks or exposed parts of boulders (Molaro et al., 2015) such that a global simulation of thermal fatigue would require detailed assumptions concerning boulder size and topography. These are generally not available prior to visiting spacecraft observations. Instead, we focused on the global trend in regolith formation by thermal fatigue.

If thermal fatigue occurs at all, it will be strongest where the strongest forcing occurs, and it has been a common assumption that this is the case around the equator. However, we identify subsolar latitude, i.e. solar declination, length of night, and thermal inertia as factors determining the latitude of maximum forcing, which does not necessarily coincide with the equator. Furthermore, as the asteroid orbits the sun, solar declination changes from its maximum on one hemisphere to its minimum on the opposite hemisphere depending on the tilt of the rotational axis. The spot of maximum thermal forcing therefore oscillates around the equator inducing regolith breakdown in a latitudinal band around that spot. This band is not sharply defined as the maximum of the temperature amplitude is relatively flat, and 90% of the forcing occurs within bands of ± 10° to ± 30° around the latitude of maximum forcing. Thus, we find that 90% of the forcing can occur in surprisingly large parts of the surface. In particular, it implies that even for a very high obliquity thermal fatigue should be strongest at, but not limited to, the equator.

This is in agreement with spacecraft observations of asteroids like, e.g., the surface of asteroid (4) Vesta, which shows ponds of fine material that are distributed between +30° and −10° (Jaumann et al., 2012). On S-type asteroid (433) Eros, fine regolith is also located in circular ponds in a ± 30° band around the equator (Robinson et al., 2001). These ponds also contain boulders that were scattered over the surface by a large impact (Thomas et al., 2001) and which were subsequently eroded by thermal stress and formed fine regolith aprons around them (Dombard et al., 2010). Thermal fatigue is not necessarily limited to these craters, but it could be more efficient there as the impact created a damage zone in the surface material, thus locally lowering thermal inertia.

The eccentricity of an asteroid's orbit causes asymmetry between the northern and southern hemispheres as thermal fatigue will be stronger at perihelion. As a result, the boulders would be more degraded on one hemisphere compared to the other if the spin axis is tilted with respect to the orbital plane. Contrarily, if the spin axis is almost perpendicular to its orbital plane, as suspected for (101955) Bennu (Lauretta et al., 2015) the subsolar latitude will remain close to the equator during the entire orbit, and a particle-size dichotomy would not be expected.

Our results imply that thermal fatigue should be much less effective at the poles or in the near-polar regions between 90° and 70°. However, regolith migration and orbital evolution could obscure the regolith distribution pattern originally induced by thermal fatigue. Regolith migration could on the one hand transport fine regolith to higher latitudes, but on the other hand fast spinning asteroids could transport regolith towards the equator forming an equatorial bulge as proposed for (101955) Bennu (Scheeres, 2015). In both cases, regolith formation could be decoupled from the observed regolith distribution to some extent. Furthermore, a change of the orientation of the rotational axis would change the location of regolith formation on evolutionary time scales, such that fine regolith could be formed by thermal fatigue at locations not predicted for the observed axis orientation. An example could be the fine regolith that is present close to the poles on S-type asteroid (25143) Itokawa, where it seems likely that material was transported to high latitudes (Miyamoto et al., 2007).

The upcoming asteroid sample return missions Hayabusa2 (Tsuda et al., 2013) and OSIRIS-Rex (Lauretta et al., 2015) will provide the opportunity to observe the morphology and thermal environment of asteroids (162173) Ryugu and (101955) Bennu in-situ. Both asteroids are expected to consist of chondritic material, and while the thermal inertia of Ryugu will be estimated using a radiometer on the MASCOT lander (Grott et al., 2017; Hamm et al., 2018) as well as the Hayabusa2 orbiter's thermal infrared imager (Okada et al., 2017), Bennu's thermal inertia will be observed by OSIRIS-REx' thermal emission spectrometer (Christensen et al., 2018). Estimates of the thermal inertia will allow for deriving global maps of grainsizes (Takita et al., 2017; Sakatani et al., 2017), and the combined observations of morphological features, grainsizes, and returned samples will provide new insights into the regolith formation process on these bodies. This will enable a comparison with the theoretical predictions presented here.

Acknowledgments

This work has been supported by the JSPS Summer Program 2017, grant number SP17305. We thank the two anonymous reviewers for their helpful, constructive contributions.

References

Auger, A.-T., Groussin, O., Jorda, L., El-Maarry, M.R., Bouley, S., Séjourné, A., Gaskell, R., Capanna, C., Davidsson, B., Marchi, S., Höfner, S., Lamy, P.L., Sierks, H., Barbieri, C., Rodrigo, R., Koschny, D., Rickman, H., Keller, H.U., Agarwal, J., A'Hearn, M.F., Barucci, M.A., Bertaux, J.-L., Bertini, I., Cremonese, G., Da Deppo, V., Debei, S., De Cecco, M., Fornasier, S., Fulle, M., Gutérrez, P.J., Güttler, C., Hviid, S., Ip, W.-H., Knollenberg, J., Kramm, J.-R., Kührt, E., Küppers, M., Lara, L.M., Lazzarin, M., Lopez Moreno, J.J., Marzari, F., Massironi, M., Michalik, H., Naletto, G., Oklay, N., Pommerol, A., Sabau, L., Thomas, N., Tubiana, C., Vincent, J.-B., Wenzel, K.-P., 2018. Meter-scale thermal contraction crack polygons on the nucleus of comet 67P/Churyumov-Gerasimenko. Icarus 301, 173–188. ISSN 0019-1035. https://doi.org/10.1016/j.icarus.2017.09.037.

Čapek, D., Vokrouhlický, D., 2010. Thermal stresses in small meteoroids. A&A 519, A75.

Čapek, D., Vokrouhlický, D., 2012. Thermal stresses in small meteoroids II, effects of an insulating surface layer. A&A 539, A25.

Delbo, Marco, Libourel, Guy, Wilkerson, Justin, Murdoch, Naomi, Michel, Patrick, Ramesh, K.T., Ganino, Clément, Verati, Chrystele, Marchi, Simone, 2014. Thermal fatigue as the origin of regolith on small asteroids. Nature 508 (7495), 233–236. https://doi.org/10.1038/nature13153.

Dombard, A.J., Barmouin, Prockter, L.M., Thomas, P.C., 2010. Boulders and ponds on the asteroid 433. Eros 2 (210), 713–721. https://doi.org/10.1016/j.icarus.2010.07.006.

Eppes, MC, Willis, A, Molaro, JL, Abernathy, S., Zhou, B., 2015. Cracks in Martian boulders exhibit preferred orientations that point to solar-induced thermal stress. Nat. Commun. 6, 6712. https://doi.org/10.1038/ncomms7712.

Garcia, R.F., Murdoch, N., Mimoun, D., 2015. Micro-meteoroid seismic uplift and regolith concentration on kilometric scale asteroids. Icarus 253, 159–168. https://doi.org/10.1016/j.icarus.2015.02.014.

Grott, M., Knollenberg, J., Borgs, B., Hänschke, F., Kessler, E., Helbert, J., Maturilli, A., Müller, N., 2017. The MASCOT Radiometer MARA for the Hayabusa 2 mission. Space Sci. Rev. 208, 413–431. https://doi.org/10.1007/s11214-016-0272-1. 1–4.

Hamm, M., Grott, M., Kührt, E., Pelivan, I., Knollenberg, J., 2018. A method to derive surface thermophysical properties of asteroid (162173) Ryugu (1999JU3) from in-situ surface brightness temperature measurements. Planetary and Space Science 159,

1–10. https://doi.org/10.1016/j.pss.2018.03.017s.
Jaumann, R, Williams, D.A, Buczkowski, D.L, Yingst, R.A, Preusker, F, Hiesinger, H, Schmedemann, N, Kneissl, T, Vincent, J.B, Blewett, D.T, Buratti, B.J, Carsenty, U, Denevi, B.W, De Sanctis, M.C, Garry, W.B, Keller, H.U, Kersten, E, Krohn, K, Li, J.-Y, Marchi, S, Matz, K.D, McCord, T.B, McSween, H.Y, Mest, S.C, Mittlefehldt, D.W, Mottola, S, Nathues, A, Neukum, G, O'Brien, D.P, Pieters, C.M, Prettyman, T.H, Raymond, C.A, Roatsch, T, Russell, C.T, Schenk, P, Schmidt, B.E, Scholten, F, Stephan, K, Sykes, M.V, Tricarico, P, Wagner, R, Zuber, M.T, Sierks, H, 2012. Vesta's shape and morphology. Science 336, 687–690. https://doi.org/10.1126/science.1219122pmid:22582254.
Kuehrt, E., 1984. Temperature profiles and thermal stresses in cometary nuclei. Icarus 60, 512.
Lauretta, D.S., Bartels, A.E., Barucci, M.A., Bierhaus, E.B., Binzel, R.P., Bottke, W.F., Campins, H., Chesley, S.R., Clark, B.C., Clark, B.E., Cloutis, E.A., Connolly, H.C., Crombie, M.K., Delbó, M., Dworkin, J.P., Emery, J.P., Glavin, D.P., Hamilton, V.E., Hergenrother, C.W., Johnson, C.L., Keller, L.P., Michel, P., Nolan, M.C., Sandford, S.A., Scheeres, D.J., Simon, A.A., Sutter, B.M., Vokrouhlický, D., Walsh, K.J., 2015. The OSIRIS-REx target asteroid (101955) Bennu: constraints on its physical, geological, and dynamical nature from astronomical observations. Meteorit. Planet. Sci. 50, 834–849. https://doi.org/10.1111/maps.12353.
Luque, A., Ruiz-Agudo, E., Cultrone, G., Sebastia´n, E., Siegesmund, S, 2011. Direct observation of microcrack development in marble caused by thermal weathering. Environ. Earth Sci. 62, 1375–1386.
Miyamoto, H., Yano, H., Scheeres, D.J., et al., 2007. Regolith migration and sorting on asteroids Itokawa. Science 316 (5827), 1011–1014. https://doi.org/10.1126/science.1134390.
Molaro, J.L., Byrne, S., Langer, S.A., 2015. Grain-scale thermoelastic stresses and spatiotemporal temperature gradients on airless bodies, implications for rock breakdown. J. Geophys. Res. Planets 120, 255–277. https://doi.org/10.1002/2014JE004729.
Molaro, J.L., Byrne, S., Le, J.-L., 2017. Thermally induced stresses in boulders on airless body surfaces, and implications for rock breakdown. Icarus 294, 247–261.
Müller, T.G., Durech, J., Ishiguro, M., et al., 2017. Hayabusa-2 mission target asteroid 162173 Ryugu (1999 JU3): searching for the object's spin-axis orientation. Astronomy Astrophys. 599, A103. https://doi.org/10.1051/0004-6361/201629134.
Opeil, C.P., Consolmagno, G.J., Britt, D.T., 2010. The thermal conductivity of meteorites: new measurements and analysis. Icarus 208 (1), 449–454. https://doi.org/10.1016/j.icarus.2010.01.021.
Okada, T., Fukuhara, T., Tanaka, S., Taguchi, M., Imamura, T., Arai, T., Senshu, H., Ogawa, Y., Demura, H., Kitazato, K., Nakamura, R., Kouyama, T., Sekiguchi, T., Hasegawa, S., Matsunaga, T., Wada, T., Takita, J., Sakatani, N., Horikawa, Y., Endo, K., Helbert, J., Müller, T.G., Hagermann, A., 2017. Thermal infrared imaging experiments of C-Type asteroid 162173 Ryugu on Hayabusa2. Space Sci. Rev. 208, 255–286. https://doi.org/10.1007/s11214-016-0286-8. 1–4.
Robinson, M.S., Thomas, P.C., Veverka, J., Murchie, S., Carcich, B., 2001. The nature of ponded deposits on Eros. Nature 413 (6854), 396–400.
Sakatani, N., Ogawa, K., Iijima, Y., Arakawa, M., Honda, R., Tanaka, S., 2017. Thermal inertia model for powdered materials under vacuum based on experimental studies. AIP Adv. 7, 015310. https://doi.org/10.1063/1.4975153.
Scheeres, D.J., 2015. Landslides and mass shedding on spinning spheroidal asteroids. Icarus 247, 1–17. https://doi.org/10.1016/j.icarus.2014.09.017.
Takita, J., Senshu, H., Tanaka, S., 2017. Feasibility and accuracy of thermophysical estimation of asteroid 162173 Ryugu (1999 JU3) from the Hayabusa2 thermal infrared imager. Space Sci. Rev. 208, 287–315. https://doi.org/10.1007/s11214-017-0336-x. 1–4.
Thomas, P.C., Veverka, J., Robinson, M.S., Murchie, S., 2001. Shoemaker crater as the source of most Ejecta blocks on the asteroid 433 Eros. Nature 413, 394–396.
Tsuda, Y., Yoshikawa, M., Abe, M., Minamino, H., Nakazawa, S., 2013. System design of the Hayabusa 2 asteroid sample return mission to 1999JU3. Acta Astronaut. 91, 356–362.
Viles, H., 2010. Simulating weathering of basalt on mars and earth by thermal cycling. Geophys. Res. Lett. 37, L18201.
Yano, H., Kubota, T., Miyamoto, H., Okada, T., Scheeres, D., Takagi, Y., Yoshida, K., Abe, M., Abe, S., Barnouin-Jha, O., Fujiwara, A., Hasegawa, S., Hashimoto, T., Ishiguro, M., Kato, M., Kawaguschi, J., Mukai, T., Saito, J., Sasaki, S., Yoshikawa, M., 2006. Science 312 (5778), 1350–1353. https://doi.org/10.1126/science.1126164.
Christensen, P.R., Hamilton, V.E., Mehall, G.L., Pelham, D., O'Donnell, W., Anwar, S., Bowles, H., Chase, S., Fahlgren, J., Farkas, Z., Fisher, T., James, O., Kubik, I., Lazbin, I., Miner, M., Rassas, M., Schulze, L., Shamordola, K., Tourville, T., West, G., Woodward, R., Lauretta, D., 2018. The OSIRIS-REx Thermal Emission Spectrometer (OTES) Instrument. Space Science Review 214, 87. https://doi.org/10.1007/s11214-018-0513-6.